Original Paper *Forma*, **25**, 1–10, 2010

Complex Basin Structure and Parameter-Mismatch Induced Intermittency in Discrete-Time Coupled Chaotic Rotors

Kai Morino† and Syuji Miyazaki*

Graduate School of Informatics, Kyoto University, Kyoto 606-8501, Japan
**E-mail address: syuji@acs.i.kyoto-u.ac.jp*

(Received February 24, 2010; Accepted May 12, 2010)

Various synchronizations and related phenomena in discrete-time coupled chaotic rotors are studied by use of numerical simulations. There exist multiple attractors with different long-time averages of the phase difference. Self-similar and complex structures of the basin in the phase space are observed. The relaxation times to attractors of the complete chaos synchronization and the generalized synchronization for the unidirectionally coupled systems are found to depend on the initial conditions in a self-similar way. Similar statistics are obtained for the first passage time of the parameter-mismatch induced intermittency. Large deviation statistics of this intermittency are numerically obtained.

Key words: Chaos Synchronization, Phase Space, Basin of Attraction, Relaxation Time, Large Deviation

1. Introduction

Originating with Huygens' observation of coupled pendula, various synchronization phenomena have been studied mainly with continuous-time dynamical systems (Pikovsky *et al.*, 2001). Introducing a suitable Poincaré surface, one can obtain discrete-time dynamical system called Poincaré map. Discrete-time models are also useful for analyzing large-deviation statistics (Suetani and Horita, 1999; Horita and Suetani, 2002), singularity spectra (Hata and Miyazaki, 1997) and spectral densities (Miyazaki and Hata, 1998) of modulational intermittency also known as on-off intermittency. This phenomenon occurs, when complete synchronization, synchronization between identical chaotic oscillators (Fujisaka and Yamada, 1983; Yamada and Fujisaka, 1983), is slightly broken.

There exist various synchronization phenomena between chaotic oscillators. For a chaotic dynamical system whose *phase* and *amplitude* can be defined, one can obtain phase-synchronized and amplitude-desynchronized state between chaotic oscillators in which control parameters are slightly different. This is called chaotic phase synchronization (CPS) (Rosenblum *et al.*, 1996; Boccaletti *et al.*, 2002; Osipov *et al.*, 2003; Politi *et al.*, 2006; Hramov *et al.*, 2008).

For a unidirectionally coupled system consisting of a driving system and a response system, general synchronization (GS) is observed, in which state variables of the response system are given by a function of those of the driving system (Rulkov *et al.*, 1994; Pyragas, 1996).

Discrete-time modeling of CPS was introduced by Fujisaka and his collaborators (Fujisaka *et al.*, 2005), which is derived as follows. Starting from an equation of motion of a harmonic oscillator with a periodic external kicking:

$$\begin{cases} \dot{\psi}(t) &= p(t), \\ \tau \dot{p}(t) &= i\omega\psi(t) - p(t) \\ & \quad + F_a(\psi, \psi^*) \cdot \displaystyle\sum_{n=-\infty}^{\infty} \delta(t - t_n), \end{cases} \tag{1}$$

we integrate the equation from $t_n - \delta$ to $t_{n+1} - \delta$ and take the limit $\tau \to 0$. Thus we have the following map

$$\begin{cases} \psi_{n+1} &= e^{i\omega} f_a(\psi_n, \psi_n^*), \\ p_{n+1} &= i\omega\psi_{n+1}, \end{cases} \tag{2}$$

with

$$f_a(\psi, \psi^*) \equiv \psi_n + F_a(\psi, \psi^*), \tag{3}$$

where the symbol $*$ denotes complex conjugate. A specific choice of the function f_a yields the Ikeda map in the field of quantum optics (Ikeda, 1979). We fix the function as $f_a(\psi, \psi^*) = (a - (1 + ib)|\psi|^2)\psi$ in the following and define the amplitude r and the phase θ as $r \equiv |\psi|$ and $\theta \equiv \arg(\psi)$, respectively.

We consider the following coupled system of n oscillators $\psi^{(j)}$ ($j = 1, 2, \cdots, n$) given by Eq. (1) via the coupling term $D\psi^{(j)}$:

$$\begin{cases} \dot{\psi}^{(j)}(t) &= p^{(j)}(t), \\ \tau \dot{p}^{(j)}(t) &= i\omega_j \psi^{(j)}(t) - p^{(j)}(t) \\ & \quad + F_a(\psi^{(j)}, \psi^{(j)*}) \cdot \displaystyle\sum_{n=-\infty}^{\infty} \delta(t - t_n) \\ & \quad + D\psi^{(j)}(t), \end{cases} \tag{4}$$

where D is an operator. Rewriting the right-hand side of

†Present address: Department of Mathematical Informatics, Graduate School of Information Science and Technology, The University of Tokyo, 7-3-1 Hongo, Bunkyo-ku, Tokyo 113-8656, Japan.

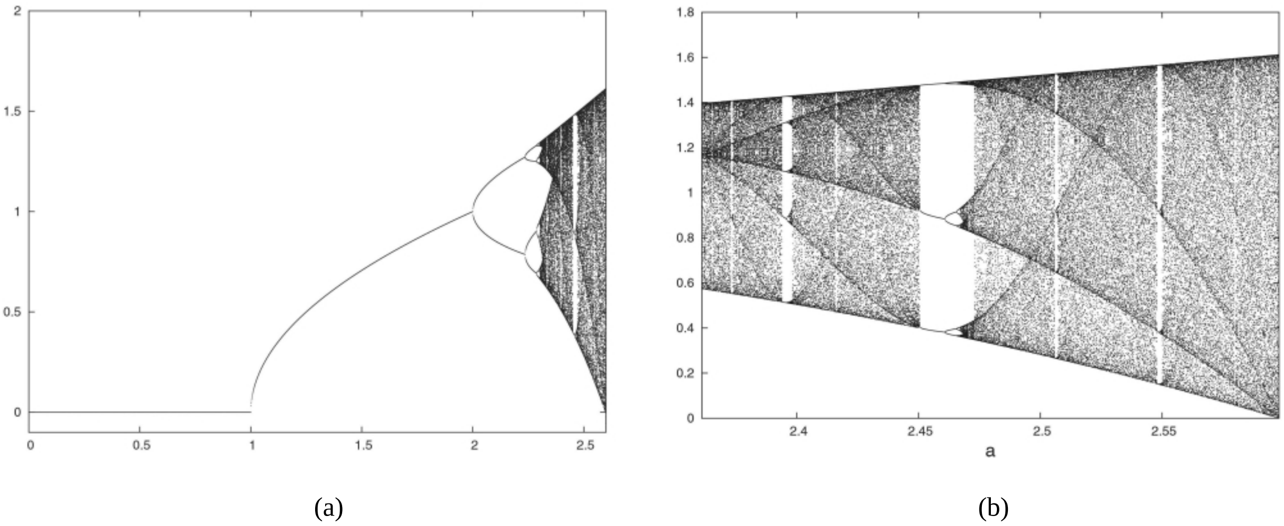

Fig. 1. Bifurcation diagrams of the amplitude $R = |\psi|$ of the single oscillator ψ plotted against the parameter a for the whole parameter range $0 \le a \le 3\sqrt{3}/2$ in (a) and for the single-band range $2.361 \le a \le 3\sqrt{3}/2$ in (b). Chaotic bands and periodic windows are observed.

Eq. (4), we have

$$\tau \dot{p}^{(j)}(t) = (i\omega_j + D)\psi^{(j)}(t) - p^{(j)}(t) \tag{5}$$

$$+ F_a(\psi^{(j)}, \psi^{(j)*}) \cdot \sum_{n=-\infty}^{\infty} \delta(t - t_n). \tag{6}$$

Integration from $t_n - \delta$ to $t_{n+1} - \delta$ and the limit $\tau \to 0$ yield

$$\begin{cases} \psi_{n+1}^{(j)} &= e^{i\omega_j + D} f_{a_j}(\psi_n^{(j)}, \psi_n^{(j)*}), \\ p_{n+1}^{(j)} &= (i\omega_j + D)\psi_{n+1}^{(j)}. \end{cases} \tag{7}$$

Let $g_j(\phi^{(j)})$ be a function of the state variable $\phi^{(j)}$ of the j-th oscillator. The coupling term is given by $Dg_j = \sum_k B_{jk} g_k$ with coefficients B_{jk}. We define the matrix $\hat{\Lambda}$ in the following relation

$$(i\omega_j + D)g_j = \sum_{k \ne j} B_{jk} g_k + (i\omega_j + B_{jj})g_j \tag{8}$$

$$\equiv \sum_k \Lambda_{jk} g_k, \tag{9}$$

where Λ_{jk} is the (j,k) component of $\hat{\Lambda}$. We also define the coefficients J_{jk} in the following relation:

$$e^{i\omega_j + D} g_j = \sum_k (e^{\hat{\Lambda}})_{jk} g_k = \sum_k J_{jk} e^{i\omega_k} g_k. \tag{10}$$

In the following, we confine ourselves to a coupled system $(\psi_n^{(1)}, \psi_n^{(2)})$ consisting of two elements. The instant phase difference $\Delta\theta_n$ is given by $\Delta\theta_n \equiv \theta_n^{(1)} - \theta_n^{(2)}$. We define the average frequency difference $\Delta\Omega$ as

$$\Delta\Omega \equiv \lim_{T\to\infty} (\Delta\theta_T - \Delta\theta_0)/T. \tag{11}$$

And we define the CPS as the state satisfying

$$\Delta\Omega = 0. \tag{12}$$

The average value of the phase difference $\Delta\theta_n$ obeys

$$\langle \Delta\theta_n \rangle = \Delta\theta_0 + \Delta\Omega \cdot n, \tag{13}$$

where $\langle \cdots \rangle$ is the statistical average over an ensemble.

In Sec. 2, we introduce discrete-time coupled chaotic rotors as a model we analyze. In Sec. 3, we consider multiple attractors and complex basin structures related to the CPS. Relations between relaxation times and complex basin structures are described in Sec. 4. Similar relations in the parameter-mismatch induced intermittency are discussed in Sec. 5. The final section is devoted to concluding remarks.

2. Discrete-Time Coupled Chaotic Rotors

In this section, we show various dynamical forms of the CPS and their relation to the Lyapunov spectra for unidirectional and bidirectional couplings. We set in the following as $\omega_1 = 0.11, \omega_2 = 0.03$, $\Delta\omega \equiv \omega_1 - \omega_2 = 0.08$, and $b = 0$. This setting always yields phase-coherent oscillations, which is different from phase-coherent or phase-incoherent Rössler oscillations (Osipov *et al.*, 2003).

For a single oscillator ψ_n under the above parameter setting, the temporal evolution of the amplitude $R_n \equiv |\psi_n| \ge 0$ is independent of the phase dynamics $\theta_{n+1} = \theta_n + \omega$ and governed by the unimodal mapping $R_{n+1} = (a - R_n^2)R_n$ from the interval $I = [0, \sqrt{a}]$ into I, which takes the local maximum value at $R = \sqrt{a/3}$. The fixed point $R = 0$ always exists. The other fixed point $R = \sqrt{a-1}$ in I exists for $a \ge 1$. The periodic points with period two $R = \sqrt{\frac{a \pm \sqrt{a^2-4}}{2}}$ in I exist for $a \ge 2$. The bifurcation diagram of the amplitude against the parameter a is shown in Fig. 1. At $a \simeq 2.314815$ and at $a \simeq 2.36089376$ four chaotic bands are merged into two bands and two bands into a single band, respectively. The attractor is destructed at $a = 3\sqrt{3}/2 \simeq 2.598$, where the trajectory starting at $R_0 = \sqrt{a}/3$ goes to the local maximum $R_1 = \sqrt{a}$, and then collides with the unstable fixed point $R_2 = 0$. One of the Lyapunov exponents is always zero which comes from the marginal phase dynamics $\theta_{n+1} = \theta_n + \omega$. The sign of the rest Lyapunov exponent is determined by the dynamics of R_n, which is controlled by the parameter a.

2.1 Unidirectional coupling

In the case of a unidirectional coupling from $\psi^{(1)}$ to $\psi^{(2)}$, the coupling term is given by $D\psi^{(1,2)} = 0$, $K(\psi^{(1)} - \psi^{(2)})$ and the coupling matrix $\hat{\Lambda}$ by

$$\hat{\Lambda} = \begin{pmatrix} i\omega_1 & 0 \\ K & i\omega_2 - K \end{pmatrix}, \tag{14}$$

where K and K_c are the coupling constant and that at the CPS transition point, respectively. Integration of Eq. (4) from $t_n - \delta$ to $t_{n+1} - \delta$ for this unidirectional coupling yields the following iterative mapping in the limit of $\tau \to 0$

$$\begin{cases} \psi^{(1)}_{n+1} &= e^{i\omega_1} f_{a_1}(\psi^{(1)}_n, \psi^{(1)*}_n), \\ \psi^{(2)}_{n+1} &= A(\Delta\omega)(1 - e^{-K - i\Delta\omega}) e^{i\omega_1} f_{a_1}(\psi^{(1)}_n, \psi^{(1)*}_n) \\ &\quad + e^{-K} e^{i\omega_2} f_{a_2}(\psi^{(2)}_n, \psi^{(2)*}_n), \end{cases} \tag{15}$$

with $A(\Delta\omega) \equiv K(K - i\Delta\omega)/(K^2 + (\Delta\omega)^2)$. For $K \to \infty$, we have $\psi^{(2)}_{n+1} \to e^{i\omega_1} f_{a_1}(\psi^{(1)}_n) = \psi^{(1)}_{n+1}$ i.e., two oscillators coincide with each other.

Defining $\hat{\psi}_n \equiv \psi_n \exp(-in\omega_1)$, we can rewrite Eq. (15) as

$$\begin{cases} \hat{\psi}^{(1)}_{n+1} &= f_{a_1}(\hat{\psi}^{(1)}_n, \hat{\psi}^{(1)*}_n), \\ \hat{\psi}^{(2)}_{n+1} &= A(\Delta\omega)(1 - e^{-K - i\Delta\omega}) f_{a_1}(\hat{\psi}^{(1)}_n, \hat{\psi}^{(1)*}_n) \\ &\quad + e^{-K} e^{-i\Delta\omega} f_{a_2}(\hat{\psi}^{(2)}_n, \hat{\psi}^{(2)*}_n), \end{cases} \tag{16}$$

where the relation $|\hat{\psi}_n| = |\psi_n|$ is used. One of the four Lyapunov exponents is always zero as a result of the marginal phase dynamics of the driving system $\hat{\psi}^{(1)}_n$. Let $\bar{\psi}$ be complex conjugate of $\hat{\psi}$. Complex conjugate of Eq. (16) yields

$$\begin{cases} \bar{\psi}^{(1)}_{n+1} &= f_{a_1}(\bar{\psi}^{(1)}_n, \bar{\psi}^{(1)*}_n), \\ \bar{\psi}^{(2)}_{n+1} &= A(-\Delta\omega)(1 - e^{-K + i\Delta\omega}) f_{a_1}(\bar{\psi}^{(1)}_n, \bar{\psi}^{(1)*}_n) \\ &\quad + e^{-K} e^{i\Delta\omega} f_{a_2}(\bar{\psi}^{(2)}_n, \bar{\psi}^{(2)*}_n), \end{cases} \tag{17}$$

where the relation $A(\Delta\omega)^* = A(-\Delta\omega)$ and the fact that the function f is ψ multiplied by a function of $|\psi|$ only are used. Substituting $\Delta\omega$ by $-\Delta\omega$ and $\bar{\psi}$ by $\hat{\psi}$ in the above equations, we have Eq. (16) again, so that by the replacement between the driving system and the response system ($\omega_1 = 0.03, \omega_2 = 0.11, \Delta\omega = -0.08$) the Lyapunov spectrum and the CPS transition point remain intact.

2.2 Bidirectional coupling

We consider here a symmetric interaction between two oscillators $\psi^{(1)}$ and $\psi^{(2)}$, where the coupling term Eq. (4) is given by $Dg_{1,2} = (K/2)(g_{2,1} - g_{1,2})$, and $\hat{\Lambda}$ satisfies

$$\hat{\Lambda} = \begin{pmatrix} i\omega_1 - \dfrac{K}{2} & \dfrac{K}{2} \\ \dfrac{K}{2} & i\omega_2 - \dfrac{K}{2} \end{pmatrix} \tag{18}$$

so that the integration of Eq. (4) from $t_n - \delta$ to $t_{n+1} - \delta$ and the limit $\tau \to 0$ yield

$$\begin{cases} \psi^{(1)}_{n+1} &= J_K(\omega_1 - \omega_2) e^{i\omega_1} f_{a_1}(\psi^{(1)}_n, \psi^{(1)*}_n) \\ &\quad + J'_K(\omega_1 - \omega_2) e^{i\omega_2} f_{a_2}(\psi^{(2)}_n, \psi^{(2)*}_n), \\ \psi^{(2)}_{n+1} &= J'_K(\omega_2 - \omega_1) e^{i\omega_1} f_{a_1}(\psi^{(1)}_n, \psi^{(1)*}_n) \\ &\quad + J_K(\omega_2 - \omega_1) e^{i\omega_2} f_{a_2}(\psi^{(2)}_n, \psi^{(2)*}_n) \end{cases} \tag{19}$$

with

$$J_K(\Delta\omega) \equiv e^{-\frac{i}{2}\Delta\omega} e^{-\frac{K}{2}} \times \left[\cosh \frac{\sqrt{K^2 - (\Delta\omega)^2}}{2} + i\Delta\omega \frac{\sinh \dfrac{\sqrt{K^2 - (\Delta\omega)^2}}{2}}{\sqrt{K^2 - (\Delta\omega)^2}} \right], \tag{20}$$

$$J'_K(\Delta\omega) \equiv e^{\frac{i}{2}\Delta\omega} e^{-\frac{K}{2}} \frac{K \sinh \dfrac{\sqrt{K^2 - (\Delta\omega)^2}}{2}}{\sqrt{K^2 - (\Delta\omega)^2}}, \tag{21}$$

which have the following symmetries

$$J_k(-\Delta\omega) = J_k(\Delta\omega)^*, \tag{22}$$

$$J'_k(-\Delta\omega) = J'_k(\Delta\omega)^*. \tag{23}$$

3. Multiple Attractors and Complex Basin Structure

A dissipative dynamical system may have multiple attractors. For example, the Lorenz model $\dot{x} = p(-x + y), \dot{y} = x(r - z) - y, \dot{z} = xy - bz$ for $13.926 < r < 24.06$, $b = 8/3$ and $p = 10$ has two stable fixed points $(x_\pm, y_\pm, z_*) = (\pm\sqrt{b(r-1)}, \pm\sqrt{b(r-1)}, r - 1)$ and an unstable chaotic invariant set (Strogatz, 1994). In Fig. 2, we plot initial points $(x(0), y(0))$ corresponding to one attractor, in which we fix as $z(0) = r - 1$ with $r = 18$, $b = 8/3$ and $p = 10$. We see that the phase space is distinguished in black and white respectively for the stable fixed points $x_- = y_- = -\sqrt{b(r-1)}$ and $x_+ = y_+ = \sqrt{b(r-1)}$ and the boundary has self-similar structure.

In our mapping model of CPS with a bidirectional coupling, similar complex structure of basin of attraction is observed. There exist multiple attractors with different long-time averages of the phase difference $\langle\Delta\theta\rangle$ for some ranges of the parameter. For $a = 2.39$ and $K = 0.10$, we have two attractors with two different long-time averages $\langle\Delta\theta\rangle \simeq 0.92$ and $\langle\Delta\theta\rangle \simeq 0.76$. In order to simplify our numerical simulation, we fix initial points of $\psi^{(1)}$ as $\psi^{(1)} = 1$, and plot initial points satisfying $\langle\Delta\theta\rangle < 0.766$ on the complex plane of $\psi^{(2)}$ in Fig. 3. We observe self-similarity structure with respect to the origin and fractal basin boundaries.

Four attractors coexist for $a = 2.39$ and $K = 0.8003$, where four different long-time averages of the phase difference are $\langle\Delta\theta\rangle = 1.051$, 1.364, 1.507 and 1.543. In Fig. 4, initial points corresponding to three attractors with $\langle\Delta\theta\rangle = 1.051$, 1.364 and 1.507 are plotted respectively in black, dark gray, and light gray. Basin of the rest attractor with $\langle\Delta\theta\rangle = 1.543$ corresponds to white regions. Complex structures in a self-similar way are clearly shown.

Our numerical results imply that unstable strange invariant sets would exist in our coupled rotors as shown in the Lorenz model.

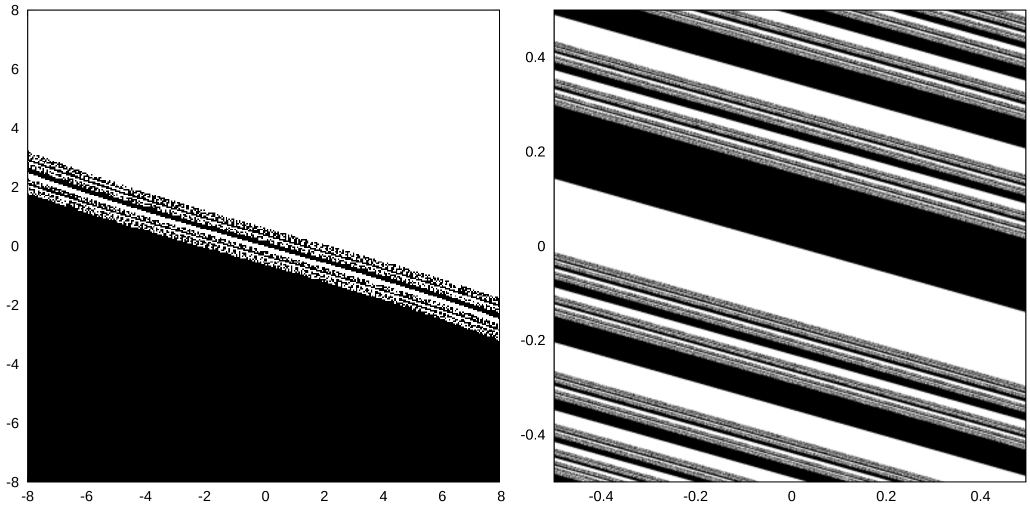

(a) (b)

Fig. 2. Initial points $(x(0), y(0))$ corresponding to one fixed point $x_- = y_- = -\sqrt{b(r-1)}$ are plotted, in which we fix as $z(0) = r - 1$ for $r = 18$, $b = 8/3$ and $p = 10$ in the Lorenz model. (b) is a blowup of (a).

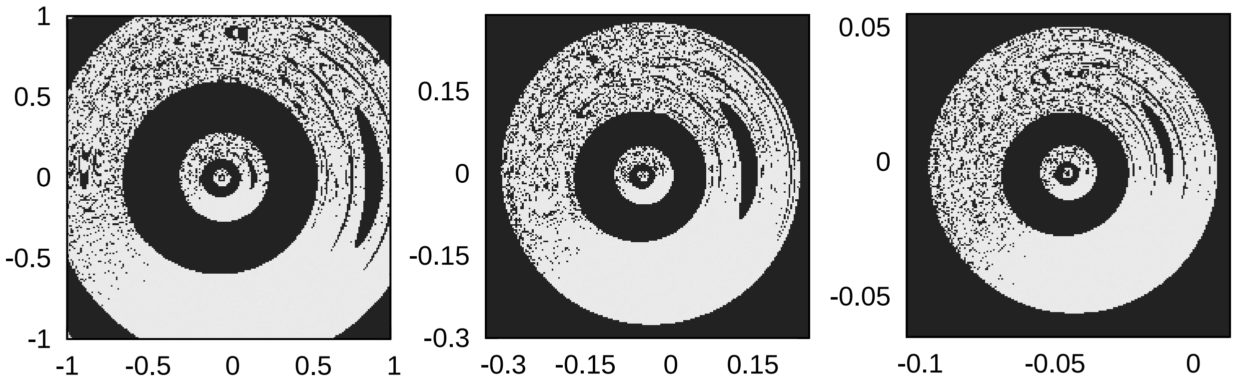

(a) (b) (c)

Fig. 3. Initial points satisfying $\langle \Delta\theta \rangle < 0.766$ on the complex plane $(\Re\{\psi_0^{(2)}\}, \Im\{\psi_0^{(2)}\})$ within the region $[-1, 1] \times [-1, 1]$ are plotted in (a) for $a = 2.39$, $K = 0.10$, and the fixed initial condition $\psi_0^{(1)} = 1$. (b) and (c) are respectively blowups of (a) and (b) with respect to the origin of the plane, where the area $[-0.33, 0.27] \times [-0.30, 0.30]$ is shown in (b) and $[-0.105, 0.015] \times [-0.065, 0.055]$ in (c).

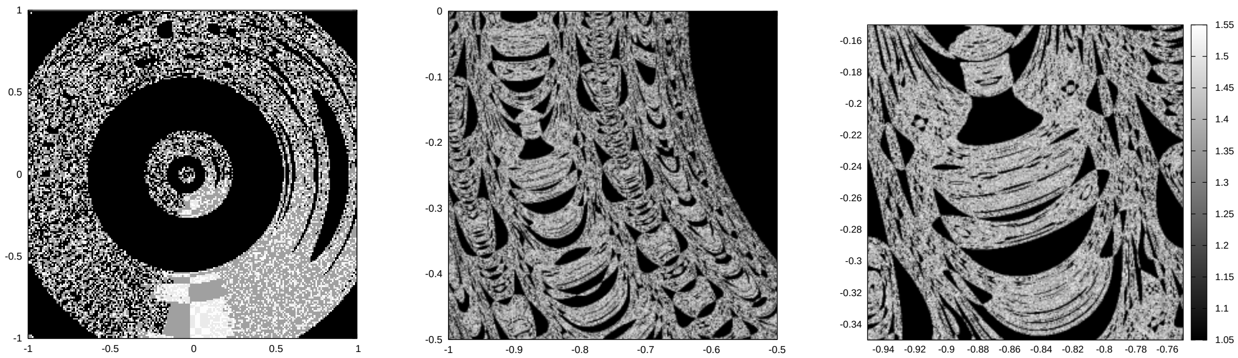

(a) (b) (c)

Fig. 4. Initial points $(\Re\{\psi_0^{(2)}\}, \Im\{\psi_0^{(2)}\})$ corresponding to three attractors are plotted in black ($\langle \Delta\theta \rangle = 1.051$), dark gray (1.364), and light gray (1.507) for $a = 2.39$, $K = 0.8003$, and the fixed initial condition $\psi_0^{(1)} = 1$. Basin of the rest attractor corresponds to white regions ($\langle \Delta\theta \rangle = 1.543$). Plotted areas in (a), (b) and (c) are respectively $[-1, 1] \times [-1, 1]$, $[-1.0, -0.5] \times [-0.5, 0]$ and $[-0.95, -0.75] \times [-0.35, -0.15]$.

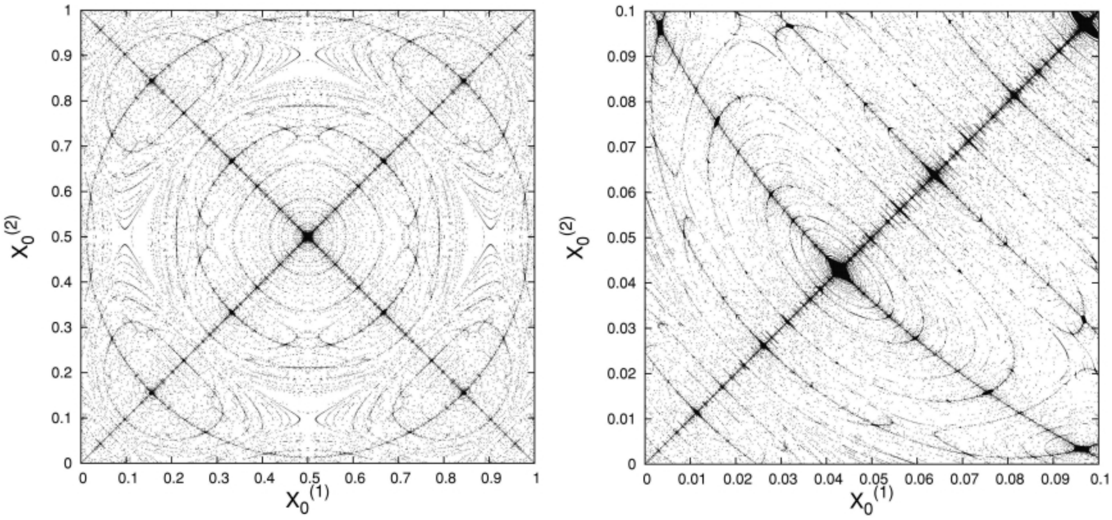

(a) (b)

Fig. 5. $(X_0^{(1)}, X_0^{(2)})$ for $a = 3.8$ and $D = 0.433$ in Eq. (24) are plotted, when $|X_n^{(1)} - X_n^{(2)}|$ becomes smaller than the threshold $l_c = 10^{-3}$ within 20 steps in (a). (b) is a blowup of (a).

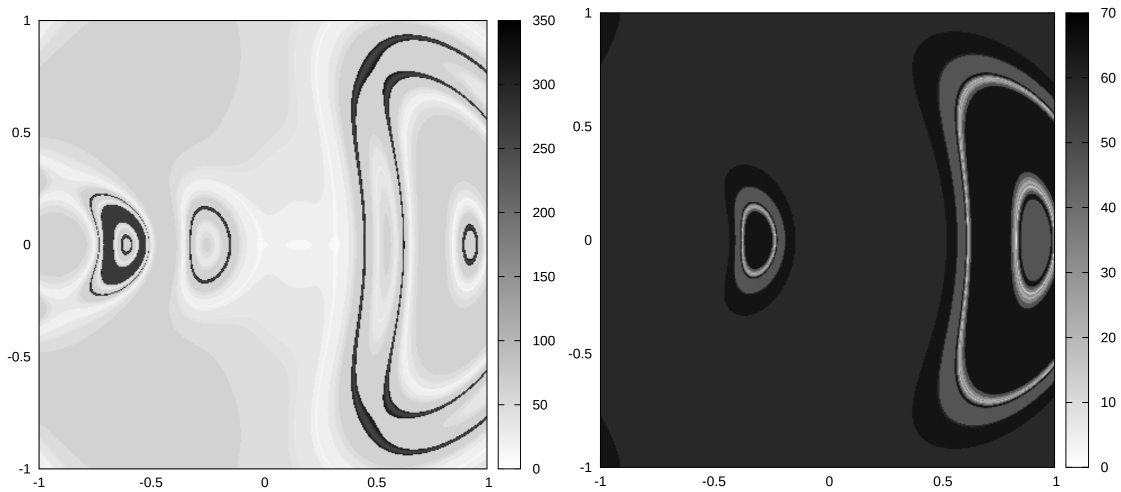

(a) $a = 2.56$ and $K = 0.6$ (b) $a = 2.52$ and $K = 0.55$

Fig. 6. Relaxation time n satisfying $|\psi_n^{(2)} - \psi_n^{(1)}| < 10^{-3}$ as a first passage time of initial points $(\Re(\psi_0^{(2)}), \Im(\psi_0^{(2)}))$ to the complete chaos synchronization are plotted in a gray scale for $a = 2.56$ and $K = 0.6$ in (a), $a = 2.52$ and $K = 0.55$ in (b).

4. Relaxation Times and Complex Basin Structure

For the logistic map $f(x) = ax(1-x)$, a bidirectionally coupled system consisting of two identical chaotic oscillators $X^{(1)}$ and $X^{(2)}$

$$\begin{cases} X_{n+1}^{(1)} &= f(X_n^{(1)}) + K[f(X_n^{(2)}) - f(X_n^{(1)})], \\ X_{n+1}^{(2)} &= f(X_n^{(2)}) + K[f(X_n^{(1)}) - f(X_n^{(2)})] \end{cases} \quad (24)$$

is considered, where K and D respectively denote the coupling strength and the largest Lyapunov exponent of the logistic map with $K = (1 + \exp(-D))/2$. For large enough K, the complete chaos synchronization occurs (Fujisaka and Yamada, 1983; Yamada and Fujisaka, 1983). In Fig. 5, initial points $(X_0^{(1)}, X_0^{(2)})$ for $a = 3.8$ and $D = 0.433$ are plotted, when the difference $|X_n^{(1)} - X_n^{(2)}|$ becomes smaller than the threshold $l_c = 10^{-3}$ within 20 steps with numerical iterations of Eq. (24) (this result has not reported in any original paper, but first published in the following tutorial paper: Fujisaka *et al.*, 1996). Relaxation times to an attractor of the complete chaos synchronization are found to depend on the initial condition in the phase space in a complex and self-similar way, which is similar to riddled basin structure with multiple attractors (Alexander *et al.*, 1992; Ott *et al.*, 1994). However, it should be noted that the complete chaos synchronization of our system has a single attractor.

For a unidirectionally coupled system consisting of the driving system $\psi^{(1)}$ and the response system $\psi^{(2)}$, complete chaos synchronization is achieved by changing the coupling strength. In Fig. 6, we plot relaxation times of initial points

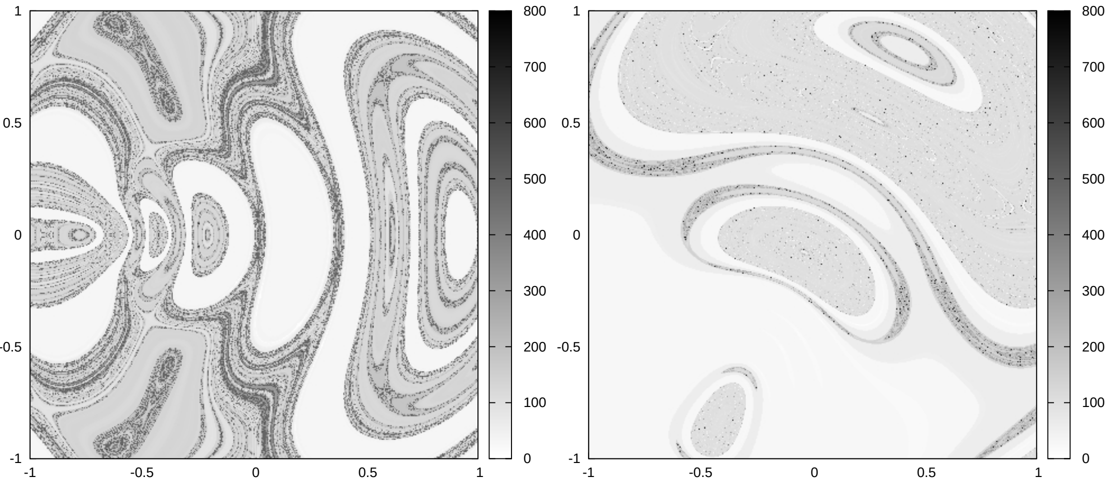

(a) $\psi_0^{(1)} = 1, \tilde{\psi}_0^{(2)} = 0.2 - 0.4i$ (b) $\psi_0^{(1)} = 0.3 + 0.6i, \tilde{\psi}_0^{(2)} = 0.2 - 0.4i$

Fig. 7. Relaxation time n satisfying $|\psi_n^{(2)} - \tilde{\psi}_n^{(2)}| < 10^{-3}$ as a first passage time are plotted in a gray scale on the phase plane $(\Re(\psi_0^{(2)}), \Im(\psi_0^{(2)}))$ for $a = 2.56$, $K = 0.5$ and $\Delta\omega = 0$ in the case of GS. (a) $\psi_0^{(1)} = 1$, $\tilde{\psi}_0^{(2)} = 0.2 - 0.4i$, (b) $\psi_0^{(1)} = 0.3 + 0.6i$, $\tilde{\psi}_0^{(2)} = 0.2 - 0.4i$.

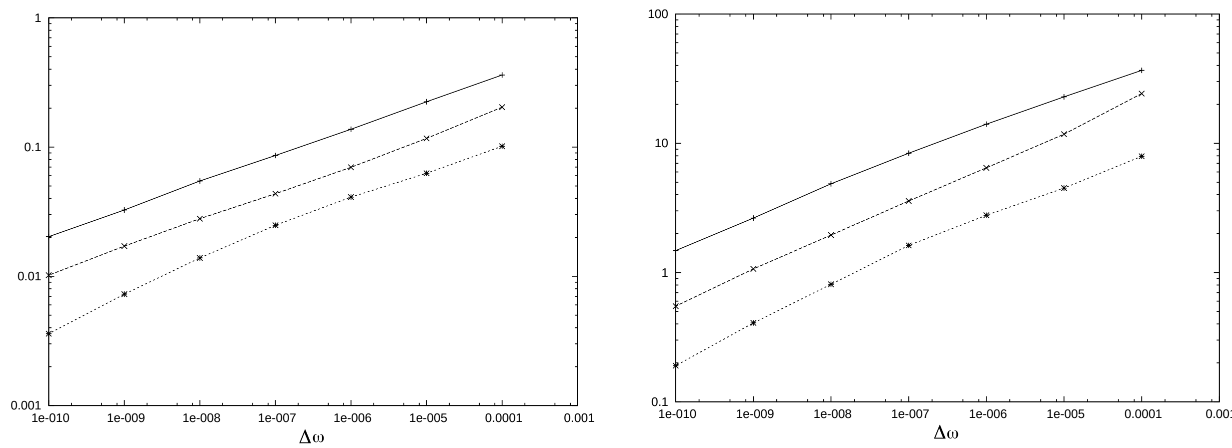

(a) $P\ (\Delta\omega)$ (b) $E\ (\Delta\omega)$

Fig. 8. $P(\Delta\omega)$ in (a) and $E(\Delta\omega)$ in (b) plotted against $\Delta\omega$ for $a = 2.56$, $K = 0.5$ and $\psi_0^{(1)} = 1$ with symbols $+$, $\times$ and $*$ corresponding to $\tilde{\psi}_0^{(2)} = 0.2 - 0.4i$, $0.2 + 0.7i$, and $-0.35 - 0.9i$, respectively.

$(\Re(\psi_0^{(2)}), \Im(\psi_0^{(2)}))$ to the complete chaos synchronization in a gray scale for $a = 2.56$ and $K = 0.6$ in (a), $a = 2.52$ and $K = 0.55$ in (b). Self-similar structures are obtained.

For the same unidirectionally coupled system consisting of the driving system $\psi^{(1)}$ and the response system $\psi^{(2)}$, GS is achieved by changing the coupling strength and a relation $\psi^{(2)} = h(\psi^{(1)})$ holds for a function $h(\cdot)$, when the second Lyapunov exponent becomes from positive to negative.

We prepare two response systems $\psi_0^{(2)}$ and $\tilde{\psi}_0^{(2)}$ with a common driving system $\psi_0^{(1)}$ in a GS state. For $n \geq n_0$ with a relaxation time n_0, $\psi_n^{(2)} = \tilde{\psi}_n^{(2)}$ is satisfied. In Fig. 7, a relaxation time n satisfying $|\psi_n^{(2)} - \tilde{\psi}_n^{(2)}| < 10^{-3}$ as a first passage time are plotted in a gray scale on the phase plane $(\Re(\psi_0^{(2)}), \Im(\psi_0^{(2)}))$ for $a = 2.56$, $K = 0.5$ and $\Delta\omega = 0$ with $(\psi_0^{(1)}, \tilde{\psi}_0^{(2)}) = (1, 0.2 - 0.4i)$ in (a) and $(\psi_0^{(1)}, \tilde{\psi}_0^{(2)}) = (0.3+0.6i, 0.2-0.4i)$ in (b). The relaxation time approaching the GS state sensitively depends on the initial condition partially in a self-similar way.

For non-vanishing phase differences $\Delta\omega$ between $\psi^{(1)}$ and $\psi^{(2)}$, GS also occurs. Let $T_{\Delta\omega}(\psi_0^{(2)})$ be relaxation time of the response system with an initial condition $\psi_0^{(2)}$ approaching the GS state for a positive phase difference $\Delta\omega > 0$. In order to measure deviations of the phase-space dependence of the relaxation time between $\Delta\omega = 0$ and $\Delta\omega > 0$, we introduce the following mean deviation $E(\Delta\omega)$ of the relaxation time and ratio $P(\Delta\omega)$ of the phase space where the relaxation time is largely changed. For numerical evaluations of $E(\Delta\omega)$ and $P(\Delta\omega)$, the phase space $(\Re(\psi_0^{(2)}), \Im(\psi_0^{(2)}))$ is divided into grids. $E(\Delta\omega)$ is given by the average over the grid points $\frac{1}{N}\sum |T_0(\psi_0^{(2)}) - T_{\Delta\omega}(\psi_0^{(2)})|$, where N is the total number of the grid points. $P(\Delta\omega)$ is evaluated as the number of grid points divided

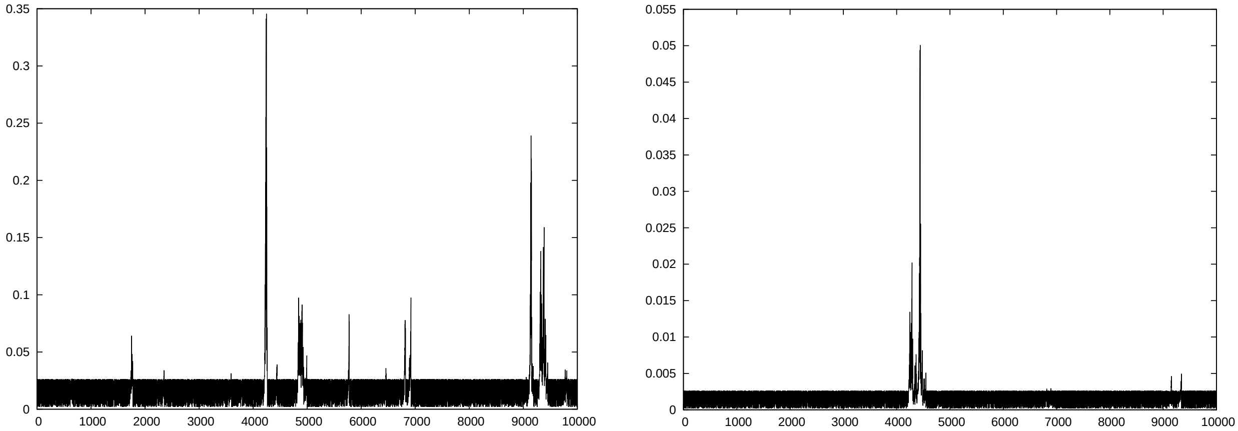

(a) $\Delta\omega = 0.01$ (b) $\Delta\omega = 0.001$

Fig. 9. Time series of $|\psi_n^{(1)} - \psi_n^{(2)}|$ with $a = 2.56$, $K = 0.6$ are plotted for $\Delta\omega = 0.01$ in (a) and 0.001 in (b).

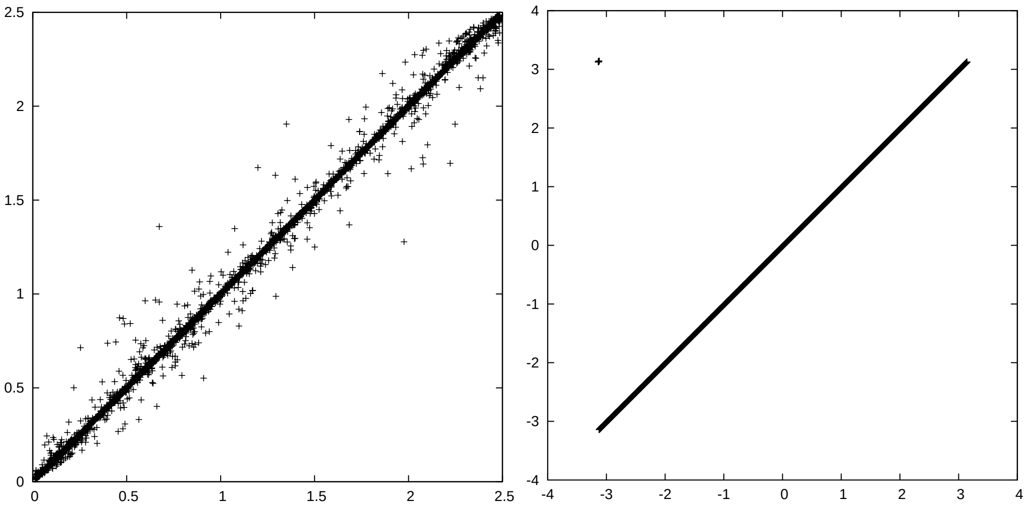

(a) $(R_n^{(1)}, R_n^{(2)})$ (b) $(\theta_n^{(1)}, \theta_n^{(2)})$

Fig. 10. (a) $(R_n^{(1)}, R_n^{(2)}) = (|\psi_n^{(1)}|, |\psi_n^{(2)}|)$ and (b) $(\theta_n^{(1)}, \theta_n^{(2)}) = (\arg\psi_n^{(1)}, \arg\psi_n^{(2)})$ for $a = 2.56$, $K = 0.6$ and $\Delta\omega = 0.01$.

by N satisfying the condition that $|T_0(\psi_0^{(2)}) - T_{\Delta\omega}(\psi_0^{(2)})|$ is smaller than a small threshold.

In Fig. 8, $P(\Delta\omega)$ and $E(\Delta\omega)$ are plotted against $\Delta\omega$ for $a = 2.56$, $K = 0.5$ and $\psi_0^{(1)} = 1$. We find algebraic dependences $P(\Delta\omega) = A\cdot(\Delta\omega)^{\alpha}$ and $E(\Delta\omega) = B\cdot(\Delta\omega)^{\beta}$ for small $\Delta\omega$, where A, B, α and β slightly depend on $\psi_0^{(1)}$ and on $\tilde{\psi}_0^{(2)}$. For $(\psi_0^{(1)}, \tilde{\psi}_0^{(2)}) = (1, 0.2 - 0.4i)$, we have $A \approx 3.5$, $B \approx 380$, $\alpha \approx 0.21$ and $\beta \approx 0.24$.

5. Parameter-Mismatch Induced Intermittency and Complex Basin Structure

Starting from the one-dimensional chaotic map $x_{n+1} = f(x_n, a)$ with a control parameter a, we consider the following unidirectionally coupled map

$$\begin{aligned} x_{n+1} &= f(x_n, a), \\ y_{n+1} &= f(y_n, a+\Delta) + D(x_{n+1} - y_{n+1}), \end{aligned} \tag{25}$$

where Δ is a small parameter mismatch. Let η be the difference $\eta = y - x$, then we have

$$\begin{aligned} \eta_{n+1} &= \frac{1}{1+D}\frac{\partial f}{\partial x}\bigg|_{\eta_n=0,\Delta=0}\eta_n \\ &\quad + \frac{1}{1+D}\frac{\partial f}{\partial a}\bigg|_{\eta_n=0,\Delta=0}\Delta, \end{aligned} \tag{26}$$

where the factor multiplied by η_n and the second term can be regarded as a multiplicative and an additive noise (Pikovsky and Grassberger, 1991) yielding an intermittent time series of η. Small and large values of $|\eta|$ are regarded as laminar and burst states of intermittent time series, respectively. The probability density function $P(\tau)$ of the laminar duration τ has an algebraic function form proportional to $\tau^{-3/2}$ for moderate values of τ and an exponential function form $\exp(-\tau/T)$ for large values of τ with a positive constant T, which is derived form a stochastic process with a multiplicative and an additive noise (Cenys *et al.*,

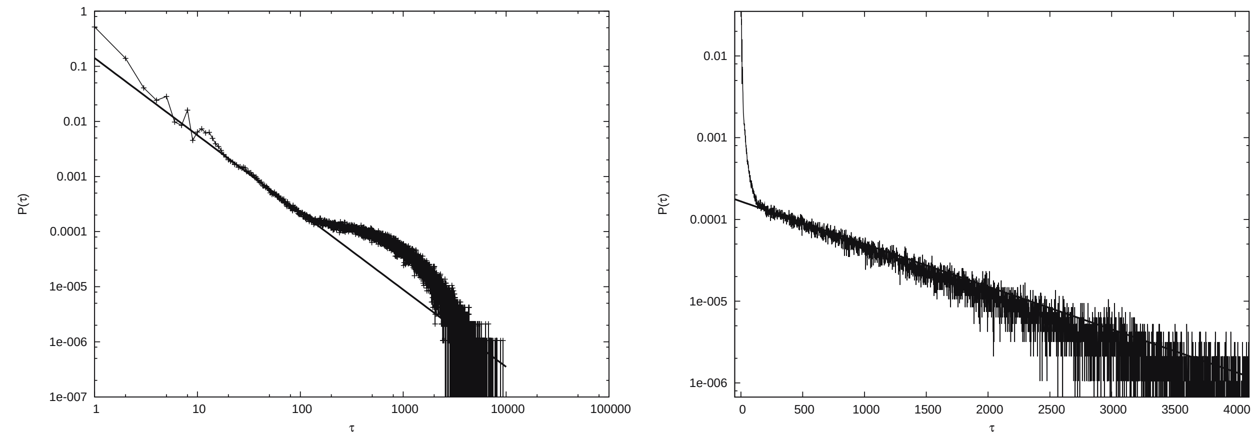

(a) Double-logarithmic plot (b) Single-logarithmic plot

Fig. 11. Distribution $P(\tau)$ of the laminar duration time τ is drawn as a double-logarithmic plot in (a) and a single-logarithmic plot in (b) for $a = 2.56$, $K = 0.6$ and $\Delta\omega = 0.01$. Functions $0.198 \times \tau^{-3/2}$ and $1.66 \times 10^{-4} \times \exp(-\tau/833)$ are respectively plotted for an eye guidance in (a) and in (b).

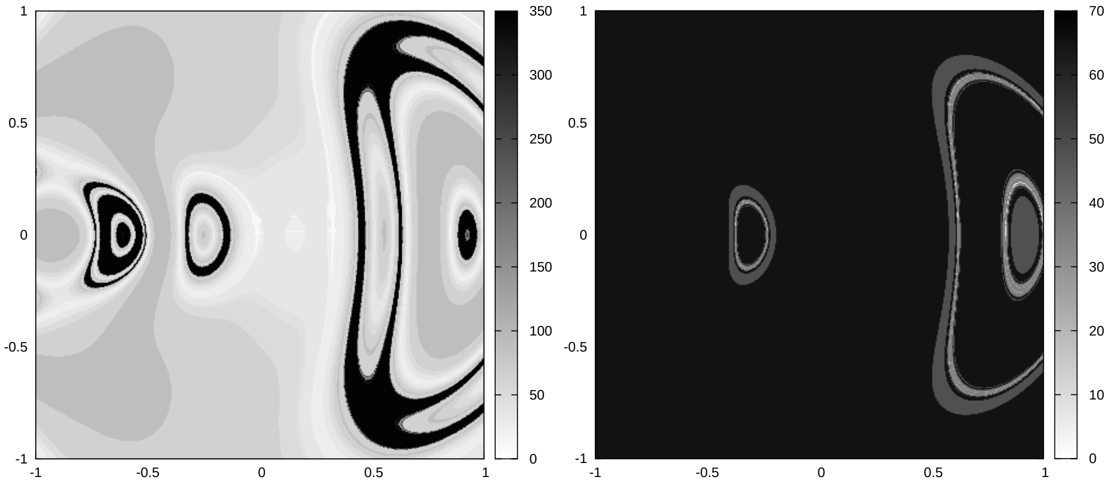

(a) $a = 2.56$ and $K = 0.6$ (b) $a = 2.52$ and $K = 0.55$

Fig. 12. Relaxation time n satisfying $|\psi_n^{(2)} - \psi_n^{(1)}| < 10^{-3}$ as a first passage time are plotted in a gray scale on the phase plane $(\Re(\psi_0^{(2)}), \Im(\psi_0^{(2)}))$ for $\psi_0^{(1)} = 1$ and $\Delta\omega = 10^{-3}$ in the case of parameter-mismatch induced intermittency. (a) $a = 2.56$ and $K = 0.6$. (b) $a = 2.52$ and $K = 0.55$.

1997).

Equation (15) with $\Delta\omega = 0$ ($\omega_1 = \omega_2$) has the complete synchronization solution $\psi^{(1)} = \psi^{(2)}$, which is stable for a strong coupling with the Lyapunov spectrum $(+, 0, -, -)$. In Figs. 9(a) and (b), time series of the difference $|\psi_n^{(1)} - \psi_n^{(2)}|$ with $a = 2.56$, $K = 0.6$ are plotted for $\Delta\omega = 0.01$ and 0.001, respectively. We confirm that these choices of the parameters satisfy the condition of the GS. As shown in Fig. 10, a solution $R^{(1)} \neq R^{(2)}$ with the phases synchronized as $\theta^{(1)} \sim \theta^{(2)}+$(small const.) appears for $\Delta\omega \neq 0$. Distributions $P(\tau)$ of laminar duration times τ keeping $|\psi_n^{(1)} - \psi_n^{(2)}| \leq 0.04$ of the time series of Fig. 9(a) are shown in Fig. 11. A distribution similar to that reported by Cenys *et al.* (1997) is obtained.

In Fig. 6(b), the relaxation time to the complete chaos synchronization as the first passage time satisfying $|\psi_n^{(1)} - \psi_n^{(2)}| < 10^{-3}$ is plotted on the plane $(\Re(\psi_0^{(2)}), \Im(\psi_0^{(2)}))$ in a gray scale for $a = 2.56$, $K = 0.6$ and $\Delta\omega = 0$. For $1 \gg \Delta\omega > 0$, the complete chaos synchronization is broken and the parameter-mismatch induced intermittency is observed. In Fig. 12, the first passage time satisfying $|\psi_n^{(1)} - \psi_n^{(2)}| < 10^{-3}$ is plotted on the plane $(\Re(\psi_0^{(2)}), \Im(\psi_0^{(2)}))$ in a gray scale for $\Delta\omega = 10^{-3}$, $\psi_0^{(1)} = 1$ and $a = 2.56$, $K = 0.6$ in (a) and $a = 2.52$ and $K = 0.55$ in (b). Note that the structure of Fig. 12 is reminiscent of that of Fig. 6(b). In order to observe quantitative structure differences, we numerically obtain $E(\Delta\omega)$ and $P(\Delta\omega)$ introduced in the preceding section, and shown in Fig. 13 for $(a, K) = (2.56, 0.6), (2.52, 0.55), (2.48, 0.45)$. Both function has an algebraic dependence on $\Delta\omega$ as $P(\Delta\omega) \approx 47.1(\Delta\omega)^{0.968}$, $E(\Delta\omega) \approx 600(\Delta\omega)^{1.12}$ for $(a, K) = (2.56, 0.6)$.

Next we study large deviation properties of the parameter-mismatch induced intermittency. For stationary discrete-time signals $\tilde{u}_j$ ($j = 1, 2, \cdots$), we consider the

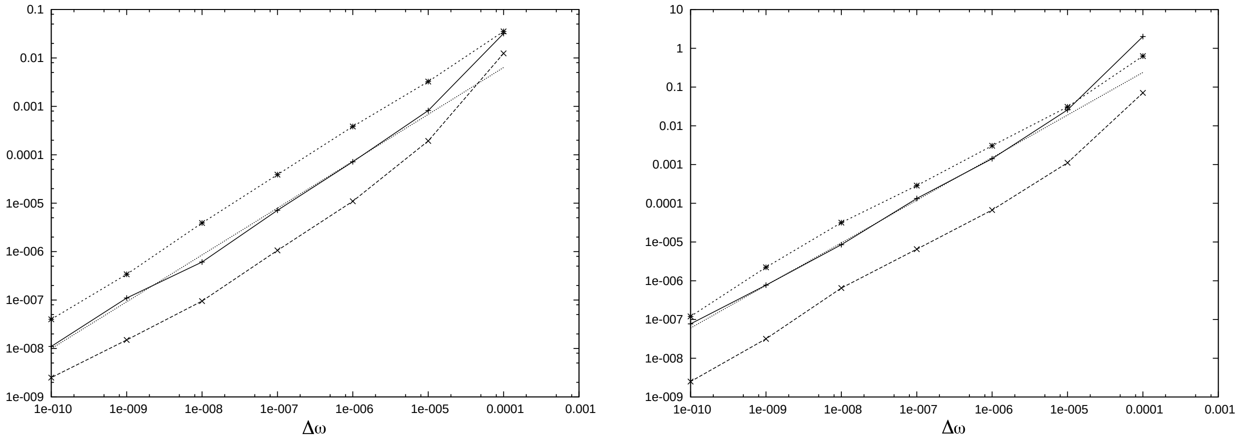

(a) $P\,(\Delta\omega)$ (b) $E\,(\Delta\omega)$

Fig. 13. $P(\Delta\omega)$ in (a) and $E(\Delta\omega)$ in (b) plotted against $\Delta\omega$ for $a = 2.56$, $K = 0.5$ and $\psi_0^{(1)} = 1$ with symbols $+$, $\times$ and $*$ corresponding to $(a, K) = (2.56, 0.6)$, $(2.52, 0.55)$, $(2.48, 0.45)$, respectively. The least mean square fitting for $(a, K) = (2.56, 0.6)$ yields $P(\Delta\omega) \approx 47.1(\Delta\omega)^{0.968}$ and $E(\Delta\omega) \approx 600(\Delta\omega)^{1.12}$ drawn by a dotted line.

following local average over n steps $\bar{u}_n = \dfrac{1}{n}\sum_{j=1}^{n}\tilde{u}_j$. For $n \to \infty$, $\bar{u}_n$ coincides with the long-time average $\langle u\rangle$. For a large but finite n, $\bar{u}_n$ fluctuates and distributes. Let the distribution function be $P_n(u)$. Even for random or chaotic time series, there exists a characteristic time scale n_c of correlation decay. For $n \gg n_c$, the following scaling holds:

$$P_n(u) \propto \exp(-nS(u)), \tag{27}$$

where $S(u)$ in Eq. (27) is called rate function or fluctuation spectrum (Fujisaka and Inoue, 1987). Note that the following limit holds:

$$P_\infty(u) = \delta(u - \bar{u}_\infty), \quad \bar{u}_\infty = \langle u\rangle\,. \tag{28}$$

The central limiting theorem around the long-time average $\langle u\rangle$ is given by the parabola $S(u) = \frac{(u-\langle u\rangle)^2}{4D}$ with the variance $2D = \langle(u - \langle u\rangle)^2\rangle$.

We first quantize the time series of Fig. 9(a) into $\tilde{u}_j = 0$ or 1 with the threshold 0.05. The correlation decay time n_c is estimated form the two-time correlation function. We choose the coarse-graining time n as $n = 2000 > n_c$. Thus, the fluctuation spectrum is shown in Fig. 14 with the parabola corresponding to the central limiting theorem. Large deviations are remarkably obtained.

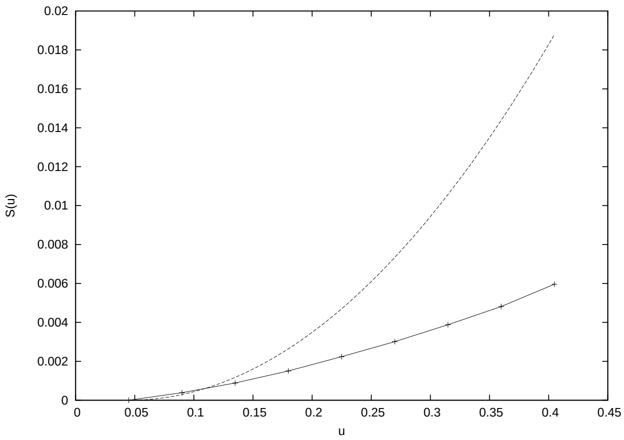

Fig. 14. Fluctuation spectrum $S(u)$ of the parameter-mismatch induced intermittency for $a = 2.56$, $K = 0.6$ and $\Delta\omega = 10^{-2}$ is plotted with the symbol $+$ combined by a solid line. Parabola corresponding to the central limiting theorem $S(u) = \frac{(u-\langle u\rangle)^2}{4D}$ with the long-time average $\langle u\rangle$ and the variance $2D$ is plotted with a dashed line. For the sake of comparison, the parabola is plotted beyond the applicable range of the central limiting theorem.

6. Concluding Remarks

In our mapping model of CPS, complex structure of basin of attraction is observed in some range of parameters. There exist multiple attractors with different long-time averages of the phase difference. We observe self-similar and complex structures of the basin in the phase space.

We also study the relaxation process to attractors of the CS and the GS. The relaxation times to attractors of the CS and the GS for the unidirectionally coupled systems are found to depend on the initial conditions in a self-similar way. In order to measure deviations of the phase-space dependence of the relaxation time between for vanishing angular velocity differences and non-vanishing ones, we introduce the mean deviation $E(\Delta\omega)$ of the relaxation time and the ratio $P(\Delta\omega)$ of the phase space where the relaxation time is largely changed. Algebraic dependences of $E(\Delta\omega)$ and $P(\Delta\omega)$ are found for small $\Delta\omega$. Similar statistics are also obtained for the first passage time of the parameter-mismatch induced intermittency.

Fluctuation spectra reflecting large deviations are numerically obtained. This result should be compared theoretical derivations of the spectra by use of the Fokker-Planck operator of a stochastic system with multiplicative and additive noise corresponding to parameter-mismatch induced intermittency.

Our discrete-time model has an advantage of studying complex basin structure over continuous-time models, which need more numerical efforts and more dimensions of the phase space. The latter also causes difficulties in a visualization standpoint.

Acknowledgments. This work was supported by a Grant-in-Aid for Scientific Research (c) (No. 20540376). We thank H. Hata, T. Horita, K. Ouchi and H. Suetani for illuminating discussions.

References

Alexander, J. C., Yorke, J. A., You, Z. and Kan, I. (1992) *Int. J. Bifur. Chaos*, **2**, 795.

Boccaletti, S., Kurths, J., Osipov, G., Valladares, D. L. and Zhou, C. S. (2002) *Physics Reports*, 366, 1.

Cenys, A., Anagnostopoulos, A. N. and Bleris, G. L. (1997) *Phys. Lett. A*, **224**, 346.

Fujisaka, H. and Inoue, M. (1987) *Prog. Theor. Phys.*, **77**, 1334.

Fujisaka, H. and Yamada, T. (1983) *Prog. Theor. Phys.*, **69**, 32.

Fujisaka, H., Fukushima, K., Inoue, M. and Yamada, T. (1996) *Butsuri* (Membership Journal of the Physical Society of Japan), **51**, 813 (in Japanese).

Fujisaka, H., Uchiyama, S. and Horita, T. (2005) *Prog. Theor. Phys.*, **114**, 289.

Hata, H. and Miyazaki, S. (1997) *Phys. Rev. E*, **55**, 5311.

Horita, T. and Suetani, H. (2002) *Phys. Rev. E*, **65**, 056217.

Hramov, A. E., Koronovskii, A. A. and Kurovskaya, M. K. (2008) *Phys. Rev. E*, **78**, 036212.

Ikeda, K. (1979) *Opt. Commun.*, **30**, 257.

Miyazaki, S. and Hata, H. (1998) *Phys. Rev. E*, **58**, 7172.

Osipov, G. V., Hu, B., Zhou, C., Ivanchenko, M. V. and Kurths, J. (2003) *Phys. Rev. Lett.*, **91**, 024101.

Ott, E., Alexander, J. C., Kan, I., Sommerer, J. C. and Yorke, J. A. (1994) *Physica D*, **76**, 384.

Pikovsky, A. S. and Grassberger, P. (1991) *J. Phys. A*, **24**, 4587.

Pikovsky, A., Rosenblum, M. and Kurths, J. (2001) *Synchronization: A Universal Concept in Nonlinear Sciences*, Cambridge University Press, Cambridge.

Politi, A., Ginelli, F., Yanchuk, S. and Maistrenko, Y. (2006) *Physica D*, **224**, 90.

Pyragas, K. (1996) *Phys. Rev. E*, **54**, R4508.

Rosenblum, M. G., Pikovsky, A. S. and Kurths, J. (1996) *Phys. Rev. Lett.*, **76**, 1804.

Rulkov, N. F., Sushchik, M. and Tsimring, L. S. (1994) *Phys. Rev. E*, **51**, 980.

Strogatz, S. H. (1994) *Nonlinear Dynamics and Chaos: With Applications to Physics, Biology, Chemistry and Engineering*, Perseus Books Publishing, Cambridge.

Suetani, H. and Horita, T. (1999) *Phys. Rev. E*, **60**, 422.

Yamada, T. and Fujisaka, H. (1983) *Prog. Theor. Phys.*, **70**, 1240.